Photoionization cross section of a hydrogenic impurity in a piezoelectric core-shell nanowire

Sihua Ha [1], Jun Zhu [2,*]

[1] College of Sciences, Inner Mongolia University of Technology, Hohhot 010051, People's Republic of China
[2] School of Physical Science and Technology, Inner Mongolia University, Hohhot 010021, People's Republic of China
*Correspondence author. Email: jiulye@126.com

ABSTRACT

The photoionization cross section (PCS) of a hydrogenic-like impurity in a piezoelectric core-shell nanowire is investigated by a variational method combined with a finite-difference algorithm. The quantum Stark effect caused by the piezoelectric field, the quantum confinement effect due to structural dimension and the electron-impurity coulombic interaction are taken into account for analyzing the photoionization properties of different types of electronic intersubband transitions. Two types of optical transitions, i.e., the transition from the impurity ground state to the unbound electron ground state and the transition between the impurity states, are involved in our numerical calculation. The PCS shows an obvious resonant peak for each optical transition, especially from the impurity high-energy states in core-shell NWs. The peak position and intensity are more sensitive to core radius than impurity position. The quantum Stark effect plays a more important role in the variation of PCS when the impurity appears in the core region but becomes less influential when the impurity moves to the shell region. Our method can be easily applied in other low-dimensional nanostructures.

Keywords: *Photoionization cross section, impurity, piezoelectric polarization, core-shell nanowire*

1. INTRODUCTION

Photoionization is one of the most fundamental processes in the interaction of light with matter which has promising applications in plasma technology, radiation protection, laser design, and radiative recombination, etc [1]. The photoionization cross section (PCS) of hydrogen-like impurities has been studied in bulk materials [2, 3] and low-dimensional nanostructures such as quantum wells (QWs) [4, 5], nanowires (NWs) [6-9], and quantum dots (QDs) [10-18]. These works have shown that the PCS, which usually has a resonant peak when the incident photon energy equals the donor binding energy, is very sensitive to impurity position, structure dimension, composition, temperature, pressure as well as external field (electric field, magnetic field, terahertz field, etc.).

To first calculate the wavefunctions and binding energies of impurities, the variational approach [2-9, 11, 12, 14, 15] with different forms of trial wavefunctions has been adopted for a coupled electron-impurity system with a confinement potential. The diagonalisation method with the use of basis function expansion [13] was sometimes employed to deal with the impurity states in multilayer nanosystems. Hu et al. [19] compared the plane wave base function expansion and variational methods for calculating the bound electronic states in low-dimensional nanostructures. Their results indicate that the two methods are qualitatively consistent and the former method is more accurate while the latter can be available in most cases. Besides the above two approaches, the finite difference (FD) [10] and finite element (FE) [16-18] numerical methods were used by some authors to directly solve the Schrödinger equation related to electron-impurity interaction.

In this work, we present a theoretical investigation on the PCS of a hydrogen-like donor impurity in a core-shell nanowire within the framework of effective mass theory. The wavefunctions and energy levels of impurities are obtained using our previously developed algorithm [20] based on FD approximation and variable principle. The piezoelectric polarization field, which may occur in epitaxial core-shell NWs due to the lattice mismatch between the core and shell materials, is taken into account according to the analytical model proposed by Boxberg et al [21]. We exemplify our numerical

U. Vandandoo et al. (eds.), *Proceedings of the International Conference on Applied Sciences and Engineering (ICASE 2023)*,
Atlantis Highlights in Engineering 22,
https://doi.org/10.2991/978-94-6463-330-6_16

computation in a coaxial cylindrical NW with a core of GaN and a shell of $Al_xGa_{1-x}N$. The influence of PCS from core radius and impurity positions is discussed in detail.

2. THEORETICAL MODEL

The schematic model of a core-shell nanowire is shown in Fig. 1. For convenience, we define a cylindrical coordinate system where the z axis is along the axis of the NW. The NW length is L and the core and shell radii are R_c and R_s, respectively. The PCS caused by the impurity states can be written according to the well-known Fermi's golden rule as

$$\sigma(\hbar\omega)=\frac{4\pi^3}{3}\alpha_{FS}\hbar\omega\left[\frac{n_r}{\varepsilon_0}\left(\frac{F_{eff}}{F_0}\right)^2\right]\times \sum_f\left|\left\langle\psi_f(\rho,\theta,z)\middle|\vec{r}\middle|\psi_i(\rho,\theta,z)\right\rangle\right|^2\delta(\Delta E_{fi}-\hbar\omega) \tag{1}$$

In above expression, $\hbar\omega$ is the incident photon energy and $\alpha_{FS}=e^2/\hbar c$ is the fine structure constant. n_r is the refractive index and ε_0 is the the static dielectric constant. F_{eff} is the effective electric field of the incident radiation on the impurity, F_0 is the average field in the medium. Since no experimental results can be found for the PCS impurity in core-shell NWs in our knowledge and the shape of the cross-section is actually not affected by the effective field ratio, the electric field ratio is taken as $F_{eff}/F_0=1$. The energy-conserving Dirac's delta function in Equation (1) can be replaced by a Lorentzian function

$$\delta(\Delta E_{fi}-\hbar\omega)\sim\frac{\hbar\Gamma_{fi}}{(\Delta E_{fi}-\hbar\omega)^2+(\hbar\Gamma_{fi})^2} \tag{2}$$

where Γ_{fi} is the hydrogenic impurity linewidth. It is worth mentioning that there are an infinite number of possible polarizations. For simplicity, we limit our calculation that the incident radiation is polarized along the z axis. Therefore, the transition matrix element of the impurity dipole moment is given by

$$M_{fi}=\left\langle\psi_f(\rho,\theta,z)\middle|ez\middle|\psi_i(\rho,\theta,z)\right\rangle \tag{3}$$

The wave functions and energy levels corresponding to the initial and final states can be obtained by solving the time-independent Schrödinger equation for an electron bound to an impurity located at (ρ_0, θ_0, z_0) in the core-shell NW. The Schrödinger equation is given as

$$\hat{H}\left|\psi(\rho,\theta,z)\right\rangle=E\left|\psi(\rho,\theta,z)\right\rangle \tag{4}$$

where the Hamiltonian in the system of electron-impurity interaction is written by

$$\hat{H}=-\frac{\hbar^2}{2m^*(\rho)}\left[\frac{\partial^2}{\partial\rho^2}+\frac{1}{\rho}\frac{1}{\partial\rho}+\frac{1}{\rho^2}\frac{\partial^2}{\partial\theta^2}\right]+V_1(\rho) -\frac{\hbar^2}{2m^*(\rho)}\frac{\partial^2}{\partial z^2}+eFz+V_2(z) -\frac{e^2}{\varepsilon_0\varepsilon(\rho)\sqrt{\rho^2+\rho_0^2-2\rho\rho_0\cos(\theta-\theta_0)+(z-z_0)^2}} \tag{5}$$

In this expression, F is the piezoelectric polarization field [21] along z-axis which is quite different for WZ and ZB crystal structures. $V_1(\rho)$ is the radial confinement potential caused by the conduction band offset between core and shell materials and $V_2(z)$ is the axial confinement potential due to vacuum level which is assumed to be infinite. The discontinuities of electronic effective mass and static dielectric constant are considered as the electron can move in the whole region of NW structure. We use a finite-difference approximation and a variational approach to solve the Schrödinger equation including the electron-impurity coulombic interaction. The trial wavefunction of impurity state is chosen as

$$\psi_{lmn}(\rho,\theta,z)=Ce^{im\theta}\phi_l(\rho)\phi_n(z) \quad e^{-\alpha\sqrt{\rho^2+\rho_0^2-2\rho\rho_0\cos(\theta-\theta_0)}}e^{-\beta(z-z_0)} \tag{6}$$

in which C is the normalization constant of the wavefunction. α and β are two variational parameters. l and n are the quantum numbers related to the radial and z-axial relative motion of an electron, respectively. The angular moment quantum number m is always taken as zero since only the light polarizations parallel and perpendicular to NW axis are taken into account in most cases. The detailed computation process can be found in our previous work [20]. Unlike most of works only discussing the transition from free electron state to impurity ground state, we will also pay close attention to the transition between impurity states. We define the unbound electron ground state as 0s, the corresponding impurity ground state as 1s with m=0, l=0, and n=0 and the impurity first excited states as $2p^+$ with m=0, l=1, and n=0, $2p^-$ with m=0, l=0, and n=1, and 2p with m=0, l=1, and n=1. Therefore, the two types of electron optical transitions, i.e., the transition from the ground state of impurity 1s to the ground state of unbound electron 0s and the transition from the first excited states of impurity ($2p^+$, $2p^-$ or 2p) to the 1s impurity state, are considered in our physical model.

3. NUMERICAL RESULTS AND DISCUSSION

We performed numerical computations on $GaN/Al_xGa_{1-x}N$ core-shell NWs (Fig. 1) with Al composition fixed at x=0.3, wire length L=10 nm and outer shell radius R_s=10 nm. In most cases, III-nitrides have two polymorphs, i.e., zinc-blende (ZB) and wurtzite (WZ) crystal structures, which show different piezoelectric polarization effect because of the polar

nature of these crystalline materials. Therefore, we considered ZB NWs grown along the [001] and [111] directions and WZ NWs grown along the [0001] direction for comparision. Due to crystalline symmetry, there is no piezoelectric polarization in ZB [001] NWs. The piezoelectric polarization in ZB [111] NWs is mainly contributed by the piezoelectric constant e_{14} whereas piezoelectric polarization in WZ[0001] NWs is caused by the piezoelectric constant e_{33}. The related material parameters used in the calculation are given in our previous work [20]. Note that the bandgap of ternary mixed crystal $Al_xGa_{1-x}N$ was calculated as $E_g(Al_xGa_{1-x}N) = xE_g(AlN) + (1-x)E_g(GaN) - bx(1-x)$ with the bowing factor b=0.6 eV while the other parameters of the $Al_xGa_{1-x}N$ were approximated by a linear interpolation method.

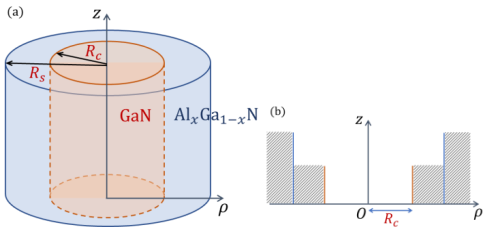

Figure 1 (a) Schematic model of a core-shell nanowire in cylindrical coordinate system where the z axis is aligned with the axis of the NWs. The radii of core GaN and outer shell $Al_xGa_{1-x}N$ are R_c and R_s, respectively. (b) Schematic radial confinement potential of a core-shell nanowire.

To evaluate the influence from the structural dimension and impurity located position on optical transitions, the transition energies related to 0s-1s ($\Delta E_{0s\text{-}1s}$), 1s-2p^+ ($\Delta E_{1s\text{-}2p+}$), 1s-2p^- ($\Delta E_{1s\text{-}2p-}$) and 1s-2p ($\Delta E_{1s\text{-}2p}$) as functions as core radius R_c and impurity radial position ρ_0 are plotted in Fig 2 and 3, respectively. It can be observed in Fig 2 that $\Delta E_{1s\text{-}2p}$ and $\Delta E_{1s\text{-}2p+}$ are larger and more sensitive to R_c than the other two no matter what crystal structure is concerned. With increasing R_c from 1 nm to 6 nm, the core area is always smaller than the shell one so that the piezoelectric polarization field in WZ [0001] and ZB [111] NWs also increases [20]. As R_c increases, $\Delta E_{1s\text{-}2p}$ and $\Delta E_{1s\text{-}2p+}$ first increase to a maximum value and then decrease monotonously. This trend changing with structural dimension can be found to be similar to that in other low-dimensional structures [4, 6, 14, 18, 19]. While the amplitude of $\Delta E_{0s\text{-}1s}$ and $\Delta E_{1s\text{-}2p-}$ changing with R_c is less than $\Delta E_{1s\text{-}2p}$ and $\Delta E_{1s\text{-}2p+}$. $\Delta E_{0s\text{-}1s}$ increases with R_c for WZ [0001] and ZB [111] NWs but decreases for ZB [001] NWs. However, $\Delta E_{1s\text{-}2p-}$ increase for ZB [111] and [001] NWs while makes less change in the case of WZ [0001] NW structure. There exist three physical mechanisms which determined the energy variation of electron intersubband transitions: (i) quantum confinement effect due to NW structure, especially along the radial direction, (ii) electron-impurity coulombic interaction, and (iii) quantum Stark effect caused by the piezoelectric polarization field. The wavefunctions of unbound and bound electron states and the average distance between the electron and impurity are determined by the synergistic effect from the three mechanisms. The piezoelectric field has an impact on the energy levels of a free electron moving along the z-axial direction but does not affect the radial movement of the electron. According to Ref. 20, the piezoelectric field in WZ [0001] NW structure is stronger than that in ZB [111] one, leading to a stronger quantum Stark effect. The radial quantum confinement on electrons changes with R_c but the axial quantum confinement keeps constant. Furthermore, the excited states of the electron or impurity, which have a larger tunneling probability through the interface between the core and shell layer, are more easily influenced by these interior quantum mechanisms. This could cause a more sensitive energy change of electron transition from these high-energy states in NWs.

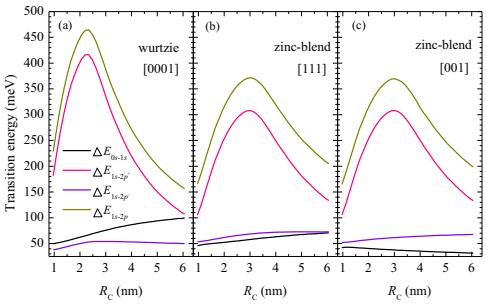

Figure 2 Transition energy as a function of the core radius R_c for the 0s-1s (black line), 1s-2p^+ (green line), 1s-2p^- (red line) and 1s-2p (blue line) transitions in a $GaN/Al_{0.3}Ga_{0.7}N$ core-shell NW for (a) [0001]-oriented WZ structure, (b) [111]-oriented ZB structure and (c) [001]-oriented ZB structure.

There is no need to consider the case of varying z_0 and θ_0 because of the symmetry of core-shell cylindrical nanowire. Fig. 3 shows that all the transition energies change a little, as the impurity locates far away from the core-center to outer shell layer. Actually, $\Delta E_{1s\text{-}2p}$, $\Delta E_{1s\text{-}2p+}$ and $\Delta E_{0s\text{-}1s}$ decrease in NWs with all the crystal structures with increasing ρ_0.

There is almost no change of $\Delta E_{1s\text{-}2p-}$ on ρ_0. That is to say, the effective distance of electron-impurity interaction becomes longer and the radial part of impurity wavefunction extends to more shell region to lower the transition energy. Compared with quantum size effect, the impurity position shows little significant impact on the transition energy.

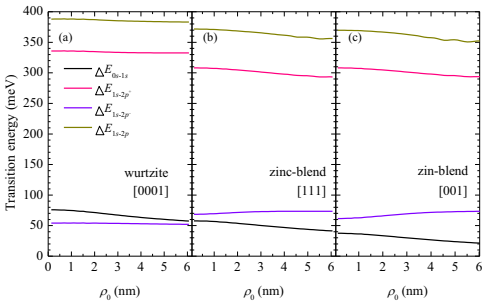

Figure 3 Transition energy as a function of the impurity radial position ρ_0 for the 0*s*-1*s* (black line), 1*s*-2p^+ (green line), 1*s*-2p^- (red line) and 1*s*-2*p* (blue line) transitions in a GaN/$Al_{0.3}Ga_{0.7}N$ core-shell NW for (a) [0001]-oriented WZ structure, (b) [111]-oriented ZB structure and (c) [001]-oriented ZB structure. The core radius R_c = 3 nm.

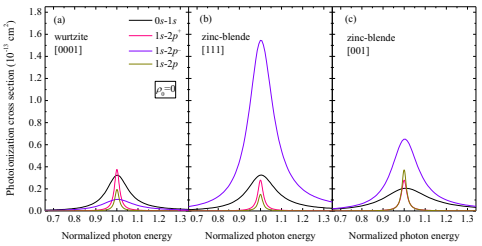

Figure 4 Photoionization cross section of the hydrogenic donor impurity located at the coordinate origin (0, 0, 0) as a function of the normalized photon energy for the 0*s*-1*s* (black line), 1*s*-2p^+ (green line), 1*s*-2p^- (red line) and 1*s*-2*p* (blue line) transitions in a GaN/$Al_{0.3}Ga_{0.7}N$ core-shell NW for (a) [0001]-oriented WZ structure, (b) [111]-oriented ZB structure and (c) [001]-oriented ZB structure. The core radius R_c = 3 nm.

Different from absorption coefficient and refractive index change which are usually studied in most literature, the PCS directly reflects the light-matter interaction. Fig. 4 gives the PCS as a function of the normalized photon energy for different types of optical transitions. The impurity is placed at the coordinate origin (0, 0, 0). The maximum of PCS is observed at the optical photoionization threshold energy and it continuously decreases as the photon energy increases or decreases from that threshold value. In other words, the PCS shows a resonant peak at $\hbar\omega$=ΔE according to Equation (2). The transition matrix element is another factor which determines the intensity of the PCS. When the impurity is at the NW center, the intensity and peak width at half height (FWHM) is different from each other. For example, the resonant peaks of 1*s*-2p^+ and 1*s*-2*p* transitions are sharper and narrower whereas the FWHM of 0*s*-1*s* and 1*s*-2p^- peaks are larger in WZ [0001] NWs. In zinc-blende, the PCS of 1*s*-2p^- transition is prominent with and without piezoelectric polarization. Others show a lower and narrower peak. It is should be mentioned that the PCS of 0*s*-1*s* transition in this work is somewhat different from the results obtained in Ref. [6-9] which demonstrated the peak position of PCS not at 1 but greater than 1. The reason may be explained that the binding energy defined in these references is underestimated due to not complete summation of free electron levels in three directions.

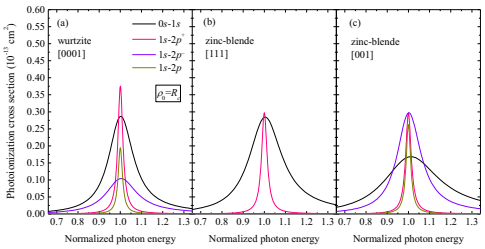

Figure 5 Photoionization cross section of the hydrogenic donor impurity located at the interface (R_c, 0, 0) as a function of the normalized photon energy for the 0*s*-1*s* (black line), 1*s*-2p^+ (green line), 1*s*-2p^- (red line) and 1*s*-2*p* (blue line) transitions in a GaN/$Al_{0.3}Ga_{0.7}N$ core-shell NW for (a) [0001]-oriented WZ structure, (b) [111]-oriented ZB structure and (c) [001]-oriented ZB structure. The core radius R_c = 3 nm.

Fig. 5 shows the PCS as a function of the normalized photon energy of different kinds of optical transitions when the impurity is placed at the interface of the core-shell nanowire. The phenomenon is different from that when the impurity is placed at the coordinate origin of NW. The PCS peak value of 1*s*-2p^+ transition in WZ [0001] NWs is larger than that in ZB [111] and [001] NWs. The PCS peak of 0*s*-1*s* becomes obvious in all the three types of NW structures. However, it can be hardly seen the peaks corresponding to 1*s*-2*p* and 1*s*-2p^- transitions in ZB [111] NWs which indicates that the overlap integral between 1*s* and 2*p* or 2p^- wavefunctions of impurity states is close to zero because of the weaker quantum confinement and stronger quantum Stark effect. There are not degenerate states and every impurity excited states can make a contribution to PCS because of the anisotropy of quantum confinement along the z-axis and radial direction. It needs to point out that all the the optical transitions between impurity states and the optical transitions between the impurity states, even impurity excited states, and unbounded electrons should be taken into account and summed to make an accurate judgment on the intensity, position and FWHM of PCS in low-dimensional quantum confined structures.

4. CONCLUSIONS

To conclude, we have made a detailed discussion on the influences of the structural dimension and impurity

position on the PCS of a hydrogenic impurity confined in a core-shell cylindrical NW. We have solved numerically the Schrödinger equation by the variational method combined with a FD approximation of partial differential equation. To assess the piezoelectric polarization effect on the electron intersubband transitions and the corresponding PCS, we took GaN/$Al_xGa_{1-x}N$ core-shell NWs with WZ crystal structure grown along [0001] direction and ZB crystal structure along [111] and [001] directions for examples. According to the numerical results, the transition energy and PCS are more sensitive to the change of core radius than impurity located position. The piezoelectric polarization field, which changes with the core radius, causes a so-called quantum Stark effect on the impurity states to shift the eigenenergy levels of a free electron moving along the *z*-axial direction. The PCS shows a resonant peak for each optical transition when the incident photon energy equals to the transition energy between two different states. The peak position and FWHM of PCS in core-shell NWs can be modulated by structural parameters as well as external conditions [7-9] if possible. Our method can be extended to any other low-dimensional quantum structures. We hope the experimental measurement of PCS for the quantum states of bound-electrons like impurities and excitons will draw extensive attention in deep exploration of the optoelectronic properties of charge carriers in low-dimensional quantum systems.

AUTHORS' CONTRIBUTIONS

J. Zhu conceived the idea and proposed the physical model of a piezoelectric core-shell nanowire. S. Ha performed the numerical calculation and data analysis. S. Ha and J. Zhu co-wrote the manuscript.

ACKNOWLEDGMENTS

This work was supported by the National Natural Science Foundation of China (Grant No. 12164031 and 62364014) and the Science Foundation of Inner Mongolia Autonomous Region (Grant No. 2020MS06007).

REFERENCES

[1] M.A. Baig, Measurement of photoionization cross-section for the excited states of atoms: A review, Atoms, 10 (2022), pp. 39. https://doi.org/10.3390/atoms10020039

[2] W. Wang, L. Gong, L. Xu, X.i Wei and S. Zhang, The effects of hydrostatic pressure and temperature on photoionization cross section of impurities in semiconductors under magnetic and intense terahertz laser fields, Opt. Mater., 111 (2021), pp. 110688. https://doi.org/10.1016/j.optmat.2020.110688

[3] W. Wang, L. Xu, X. Wei, S. Zhang, Intense-terahertz-laser modulated photoionization cross section of shallow-donor impurity in semiconductors in a magnetic field, Res. Phys., 20 (2021), pp. 103692. https://doi.org/10.1016/j.rinp.2020.103692

[4] A. Sali, M. Fliyou, L. Roubi and H. Loumrhari, The effect of a strong magnetic field on the binding energy and the photoionization cross-section in a quantum well, J. Phys.: Condens. Matter, 11 (1999), pp. 2427-2436. https://doi.org/10.1088/0953-8984/11/11/013

[5] A.L. Morales, N. Raigoza, E. Reyes-Gómez, J.M. Osorio-Guillén and C.A. Duque, Impurity-related polarizability and photoionization-cross section in GaAs/Ga1-xAlxAs double quantum wells under electric fields and hydrostatic pressure, Superlatt. Microstruct., 45 (2009), pp. 590-597. https://doi.org/10.1016/j.spmi.2009.03.001

[6] U. Yesilgul, E. Kasapoglu, H. Sari and I. Sökmen, Photoionization cross-section and binding energy of shallow donor impurities in Ga1-xInxNyAs1-y/GaAs quantum wires, Solid State Commun., 151 (2011), pp. 1175-1178. https://doi.org/10.1016/j.ssc.2011.04.029

[7] U. Yesilgul, Donor impurity-related photoionization cross-section in parabolic quantum wires: Effects of intense laser field and applied electric field, Physica E, 74 (2015), pp. 34-38. https://doi.org/10.1016/j.physe.2015.06.021

[8] A.J. Peter, E. Kasapoglu and F. Ungan, Magneto-optical properties of impurity associated photoionization cross-section in laser-driven delta-doped quantum wires, Physica B, 620 (2021), pp. 413285. https://doi.org/10.1016/j.physb.2021.413285

[9] A.J. Peter, M.E. Mora-Ramos and F. Ungan, Intense terahertz laser field induced electro-magneto-donor impurity associated photoionization cross-section in Gaussian quantum wires, Physica E, 143 (2022), pp. 115270. https://doi.org/10.1016/j.physe.2022.115270

[10] M. Sahin, F. Tek and A. Erdinc, The photoionization cross section of a hydrogenic impurity in a multi-layered spherical quantum dot, J. Appl. Phys., 111 (2012), pp. 084317. https://doi.org/10.1063/1.4705410

[11] E. Feddi, M. El-Yadri, F. Dujardin, R.L. Restrepo and C. A. Duque, Photoionization cross section and binding energy of single dopant in hollow cylindrical core/shell quantum dot, J. Appl. Phys., 121 (2017), pp. 064303. https://doi.org/10.1063/1.4975648

[12] S. M'zerd, M. El Haouari, M. Aghoutane, M. El-Yadri, E. Feddi, F. Dujardin, I. Zorkani, A. Jorio,

M. Sadoqi and G. Long, Electric field effect on the photoionization cross section of a single dopant in a strained AlAs/GaAs spherical core/shell quantum dot, J. Appl. Phys., 124 (2018), pp. 164303. https://doi.org/10.1063/1.5046859

[13] M.V. Chubrei, V.A. Holovatsky and C.A. Duque, Effect of magnetic field on donor impurity-related photoionisation cross-section in multilayered quantum dot, Phil. Mag., 101 (2021), pp. 2614-2633. https://doi.org/10.1080/14786435.2021.1979267

[14] L. Shi, Z.W. Yan and M.W. Meng, Binding energy and photoionization cross section of hydrogenic impurities in elliptic cylindrical core/shell quantum dots under a non-axial electric field, Superlatt. Microstruct., 150 (2021), pp. 106818. https://doi.org/10.1016/j.spmi.2021.106818

[15] F. Oketch and H. Oyoko, A theoretical study of the effects of Thomas-Fermi and Hermanson's dielectric functions and temperature on photoionization cross-section of a donor impurity in GaAs quantum dots of circular and rectangular cross-sections, Eur. Phys. J. B, 95 (2022), pp. 44. https://doi.org/10.1140/epjb/s10051-022-00301-4

[16] A. Fakkahi, H. Dakhlaoui, A. Sali, M. Jaouane, R. Arraoui, K. El-bakkari and A. Ed-Dahmouny, Pressure, temperature and electric field effects on the photoionization cross section in a multilayered spherical quantum dot, Eur. Phys. J. Plus, 137 (2022), pp. 1244. https://doi.org/10.1140/epjp/s13360-022-03462-4

[17] M. Jaouane, A. Sali, A. Fakkahi, R. Arraoui, A. Ed-Dahmouny and F. Ungan, Photoionization cross section of donor single dopant in multilayer quantum dots under pressure and temperature effects, Physica E, 144 (2022), pp. 115450. https://doi.org/10.1016/j.physe.2022.115450

[18] A. Fakkahi, M. Jaouane, K. Limame, A. Sali, M. Kirak, R. Arraoui, A. Ed-Dahmouny, K. El-bakkari and H. Azmi, The impact of the electric field on the photoionization cross section, polarizability, and donor impurity binding energy in multilayered spherical quantum dot, Appl. Phys. A, 129 (2023), pp. 188. https://doi.org/10.1007/s00339-023-06472-w

[19] M. Hu, H. Wang, Q. Gong and S. Wang, Electronic states in low-dimensional nano-structures:Comparison between the variational and plane wave basis method, Superlatt. Microstruct., 104 (2017), pp. 37-45. https://doi.org/10.1016/j.spmi.2017.02.006

[20] S. H. Ha and J. Zhu, Hydrogenic impurity-related optical properties in a piezoelectric core-shell nanowire, J. Appl. Phys., 128 (2020), pp. 034305. https://doi.org/10.1063/1.514522 7

[21] F. Boxberg, N. Søndergaard and H.Q. Xu, Photovoltaics with piezoelectric core-shell nanowires, Nano Lett., 10 (2010), pp. 1108-1112. https://doi.org/10.1021/nl9040934